Support-Q Optimisation of a Trapped Mode Beam Resonator

T. H. Hanley*[1], H. T. D. Grigg[1], and B. J. Gallacher[1]
[1]Newcastle University, Newcastle-Upon-Tyne
*Corresponding author: School of Mechanical and Systems Engineering, Newcastle University, Stephenson Building, Claremont Road, Newcastle upon Tyne NE1 7RU, UK, t.h.hanley@ncl.ac.uk

Abstract: The introduction of a disorder into a finite periodic oscillatory system induces the presence of a 'trapped mode': a mode in which the displacement field is localised to the region of the disorder. A main inhibitor to MEMS resonators achieving a high quality (Q) factor is energy radiation through the support to the substrate. The trapped modes present a way to tune this support loss to a minimal value and thus are a good potential candidate for a high-Q geometry. An initial geometry is proposed and contrasted to a lumped-parameter model. Separate two-dimensional resonator and substrate COMSOL models are used in combination to determine an optimal geometry for a maximum support Q (Q_{SUPP}). The Q_{SUPP} is shown to be on the order of the highest currently available in the literature. The theoretical maximum achievable Q factor, due to other dominant Q contributions, is discussed.

Keywords: MEMS, Resonant Sensors, Periodic Beam, Trapped Mode Resonator

1. Introduction

The sensitivity of MEMS resonant sensors is dependent on a high quality (Q) factor. The Q factor can be described as the sum of the forms of dissipation that contribute to it (equation 1). In MEMS devices, the most prominent of these are surface loss (Q_{SURF}), gas damping (Q_{GAS}), thermoelastic damping (Q_{TED}) and support loss (Q_{SUPP}) [1], [2].

$$Q_{TOTAL}^{-1} = Q_{SUPP}^{-1} + Q_{SURF}^{-1} + Q_{TED}^{-1} + Q_{GAS}^{-1} + Q_{OTHER}^{-1} \quad [1]$$

Q_{SUPP} is one of the dominant contributors to the overall Q of the resonator; this is quantified by equation 2 [2].

$$Q_{SUPP} = 2\,\pi\,\frac{W_n}{\Delta W} \quad [2]$$

Where W_n and ΔW are the stored energy and energy loss through the support respectively. For a beam resonator vibrating its n[th] natural frequency, ω_n, the stored energy can be described by equation 3. Where ρ, A and L are the density, cross sectional area and length of the beam respectively. U_n is the vibration amplitude [3].

$$W_n = \frac{1}{8}\rho A L \omega_n{}^2 U_n{}^2 \quad [3]$$

The energy lost through the support can be written in terms of the shear force, F_S, and the displacement field, u, at the beam-substrate interface [2]. The contribution due to the bending moment can be neglected [4].

$$\Delta W = \pi\, F_S\, u_{x=0} \quad [4]$$

The Q_{SUPP} can be optimised by designing a resonator geometry so that the oscillating force, F_S, at the support interface is minimized, and the energy stored, W_n, in the bulk of the resonator is maximized. A structure exhibiting a trapped mode would be an ideal candidate for a high Q_{SUPP} resonator. One class of finite periodic system that can exhibit trapped modes are stepped beams. These can be easily integrated into planar systems and are well suited for use as isolating tethers, wave guides, delay lines or resonant sensors.

It is commonly known that infinite periodic media possess frequency bands in which waves can either propagate (pass-bands) or where waves are attenuated (stop-bands) [5]. When the system is truncated and non-dissipative boundaries imposed, the oscillations become stationary and can be described by a superposition of modes. The modes of such a system fall within the pass bands of the infinite periodic system [6]. When a disorder is introduced, a mode is shifted into the stop band and becomes a trapped mode (figure 1).

The particular geometry of interest is elucidated in the inset of figure 1. Slender Euler-Bernoulli (EB) beams are separated by much thicker sections of the beam, which do not themselves fall within the bounds of EB assumptions.

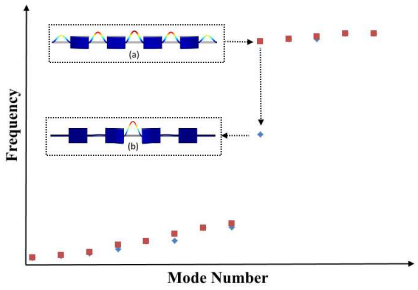

Figure 1. Dispersion plot showing frequency shift of the distributed mode (a) into the stop-band forming the 'trapped mode', (b).

It has been shown experimentally that as little as three periods of such a system excited in the stop band can enable a complete decay of the displacement field [7]. The present analysis focuses on a 4.5 period beam, with the displacement field localized to the central region (fig. 1b).

2. Lumped parameter model

2.1 Equivalent system

An equivalent lumped parameter model was employed to gain initial insight into the parameters of interest. This is presented here, along with the underlying approximations.

In the global mode shape of interest (fig. 1a) the EB beam sections will be oscillating locally in their first mode, therefore they are modelled with a single degree of freedom (DOF). This limits the analysis to the first band gap. The larger sections of the beam are assumed to experience minimal deformation. To simplify the model and reduce the DOFs, zero elastic deformation is assumed and therefore these are also modelled with one DOF.

The sections can be connected to form the full 4.5 period equivalent system of interest (fig. 2).

2.2 EVP Solution

The general non-dimensionalised eigenvalue problem for the non-localised system is given in equation 5. The form of the stiffness and mass matrices are given in equations 6.1 and 6.2 and respectively.

$$([\mathbf{K}] - \boldsymbol{\lambda}\,[\mathbf{M}])\underline{x} = [\mathbf{0}] \qquad [5]$$

$$[\mathbf{K}] = \begin{bmatrix} \mathbf{2} & \mathbf{-1} & & & & & \\ \mathbf{-1} & \mathbf{2} & \mathbf{-1} & & & & \\ & \mathbf{-1} & \mathbf{2} & & & & \\ & & & \cdot & & & \\ & & & & \cdot & & \\ & & & & & \mathbf{2} & \mathbf{-1} \\ & & & & & \mathbf{-1} & \mathbf{2} \end{bmatrix} \qquad [6.1]$$

$$[\mathbf{M}] = \begin{bmatrix} \boldsymbol{m_r} & & & & & & \\ & \mathbf{1} & & & & & \\ & & \boldsymbol{m_r} & & & & \\ & & & \cdot & & & \\ & & & & \cdot & & \\ & & & & & \mathbf{1} & \\ & & & & & & \boldsymbol{m_r} \end{bmatrix} \qquad [6.2a]$$

$$m_r = \frac{m_1}{m_2}, \qquad m_r < 1, \qquad m_r \neq 0 \qquad [6.2b]$$

A simple numerical analysis can be performed for the non-dimensional case by perturbing the stiffness matrix (the change in mass is assumed negligible). Equations 7.1-7.6 are substituted into equation 5.

$$[\mathbf{K}] = [\mathbf{K_0}] + [\boldsymbol{\delta}\mathbf{K}] \qquad [7.3]$$

$$[\boldsymbol{\delta}\mathbf{K}] = \begin{bmatrix} \mathbf{0} & & & & & & \\ & \cdot & & & & & \\ & & \boldsymbol{\delta_k} & \boldsymbol{-\delta_k} & & & \\ & & \boldsymbol{-\delta_k} & \boldsymbol{2\delta_k} & \boldsymbol{-\delta_k} & & \\ & & & \boldsymbol{-\delta_k} & \boldsymbol{\delta_k} & & \\ & & & & & \cdot & \\ & & & & & & \mathbf{0} \end{bmatrix} \qquad [7.6]$$

$$\delta_k = \frac{\Delta k}{k}, \qquad \delta_k \ll 1 \qquad [7.6b]$$

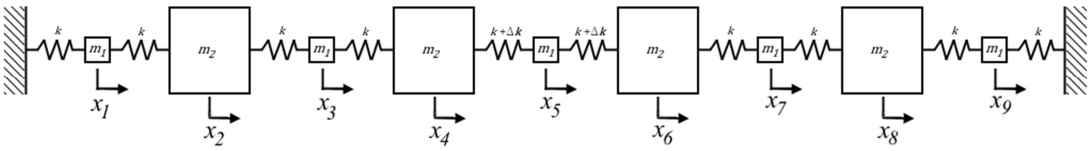

Figure 2. 4.5 period equivalent lumped parameter model.

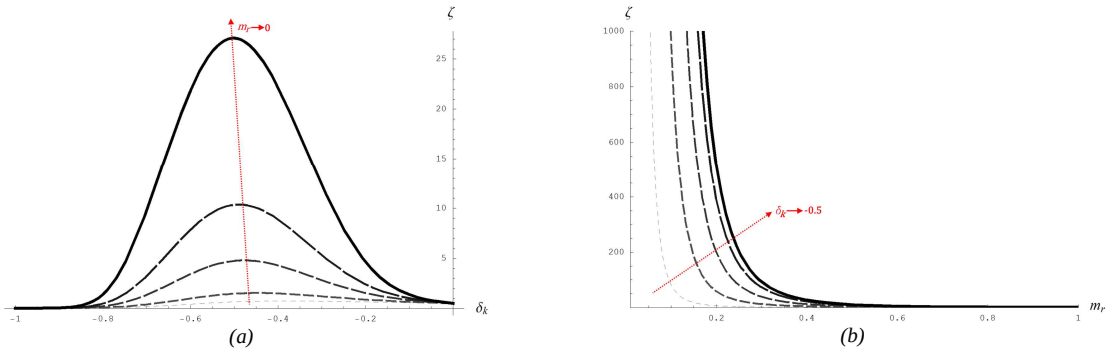

(a) *(b)*

Figure 3. Plots of energy localisation coefficient against parameters, m_r and δ_k.

A quantity is required that is comparable to Q_{SUPP}. In order to maximize Q_{SUPP}, the stored energy at the centre must be maximized and the energy at the ends minimized. Solving the perturbed EVP will yield a localised mode, x_L, from which the potential energy for the central and end masses can be calculated. The ratio of these is assumed to be proportional to the support loss. Thus, an 'energy localization coefficient', ζ, is defined by taking the ratio of the strain energy stored in the central (5th) DOF to the energy stored in the end (1st and 9th) DOFs (equation 9).

$$\zeta = \frac{(1 + \delta K)\left|x_L^{(5)}\right|^2}{\left|x_L^{(1)}\right|^2 + \left|x_L^{(9)}\right|^2} \qquad [9]$$

The change in ζ with varying mass ratio, m_r, and stiffness perturbation, δ_k, is shown in figures 3a-b. It must first be noted that the cases when either m_r = 0 or δ_k =-1 are both unphysical and are to be ignored in the analysis. It can be seen from both figures 3a and b that when $|\delta_k| > 0$, ζ asymptotically tends to infinity as as m_r approaches zero. In addition to this, figure 3b shows that the rate of change of the gradient increases with increasing δ_k. It is shown in Figure 3a that ζ approaches a maximum at an optimal value of $\delta_k \approx$ -0.5.

3. COMSOL Models

3.1 Geometries and Meshing

Two separate 2D models were used for the resonator and substrate, both using silicon material properties.

The resonator geometry (fig. 4) was halved and replaced by a symmetry boundary in the centre of the central slender beam section. This assumes that the energy loss at each boundary is equal and uncoupled. The substrate model consisted of three concentric semicircles, the smallest of which to define the loading region, and the others to define the total substrate region and a perfectly matched layer (PML).

Meshing for both models was predominantly accomplished using free quadrilateral meshing. A mapped face mesh was employed for the slender sections in the resonator model. The dimensions of the resonator geometry are summarised in table 1.

3.2 Solver

COMSOL's post processor provided a value for the stored energy. This was compared to an analytical calculation of the sum of the energy (equation 3) stored in each of the slender beam sections, with the displacement amplitudes taken from the COMSOL solution. These were found to agree to within 20%, with an average difference of 15%. The difference can most likely be attributed to energy stored in the thick beam sections that is neglected in the analytical comparison calculation.

The shear stress can also be taken directly from COMSOL, however, due to the sharp changes in cross section, an extremely fine mesh would be required to achieve a consistent result. To allow for a coarser mesh and faster computation times, the shear force was calculated from equation 4.

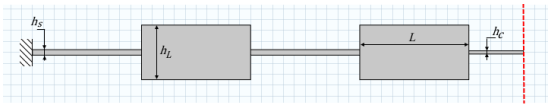

Figure 4. Tuning parameters of the resonator model. The dashed red line denotes the symmetry boundary.

Resonator Dimension Summary	
L	100 μm
h_s	5 μm
h_c	1.25 – 5 μm
h_L	50 – 100 μm

Table 1. Resonator dimensions.

A parametric sweep ran through the desired values of h_L and h_c. The required data was taken from the 5th Eigenmode output from an Eigenfrequency analysis.

The substrate model was used to quantify the energy radiated away from the resonator per cycle. Referring to equation 4 it can be seen that the displacement field across the loading region is required as output from this model. Frequency and shear load solutions gleaned from the resonator solution were input into a parametric sweep for a Frequency Domain analysis.

4. Results

The results from the COMSOL models were combined with equations 2-4 and a maximum value sought. The results are summarized by figure 4.

The maximum Q_{SUPP} achieved was ~3x10^8 which corresponded to a step thickness ratio of 20 and a disorder thickness ratio of 0.45. These values correspond to m_r = 0.05 and $\delta_k \approx$ -0.8. The contour plots (figures 5a-b) compare the COMSOL solution and the lumped parameter solution. In general, good qualitative agreement is found within the bounds of validity of the perturbation solution.

4. Discussion

4.1 Q_{SUPP} of a TMBR

Quoted values for Q_{SUPP} are sparse in the literature, however, the TMBR compares favourably to the values available. Two examples of note are for a xylophone bar resonator (XBR) [1], [8] and a micro-cantilever [2]. Contrasting these to the TMBR, the TMBR Q_{SUPP} is found to be of the same order or greater.

The numerical value given for Q_{SUPP} is dependent on the scale of the device. Therefore, it is more useful to compare the parameters affecting the Q_{SUPP} and the limits imposed by them. In the case of the TMBR the Q_{SUPP} is limited by the maximum thickness ratio, which is equivalent to the wave-speed ratio, V_R, between the segments.

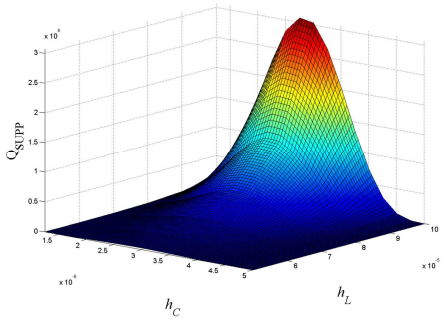

Figure 4. Q_{SUPP} with varying thickness ratio and size of disorder (h_s kept constant)

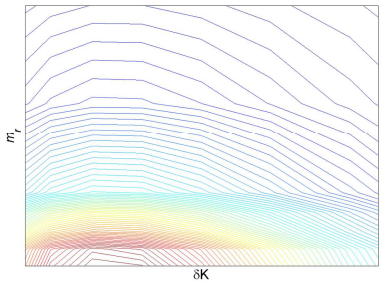

(a)

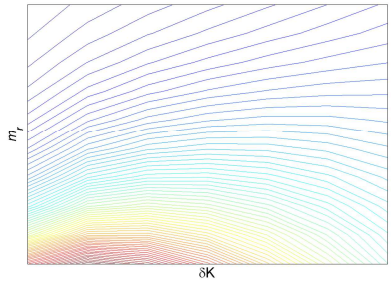

(b)

Figures 5a-b. Contour plots of the COMSOL (a) and perturbation (b) solutions for Q_{SUPP}.

Therefore, the Q_{SUPP} is limited by the mass the slender beams can support. Increasing V_R provides a simple method for increasing the Q_{SUPP} in a TMBR. The Q_{SUPP}, however, only needs to be tuned to a value where it is no longer the dominant form of dissipation. After this, efforts should be focused on reducing the new dominant dissipation mechanism to achieve the maximum Q_{TOTAL}.

4.2 Tuning for high-Q_{TOTAL}

Q_{SUPP} is limited in general by geometric factors. Tuning to optimise these may affect the other Q contributors, leading to a compromised Q_{TOTAL}. It is reasoned in this section that in the case of the TMBR, the parameters determining the other dominant Q contributors are uncoupled from the Q_{SUPP} tuning parameters.

The dominant Q contributors for a silicon MEMS resonator operating in a vacuum are Q_{SUPP}, Q_{TED} and Q_{SURF} [2]. Calculating the equivalent values of these quantities for coupled systems [8] takes advantage of the fact that both Q_{TED} and Q_{SURF} are local dissipation mechanisms [9].The Q_{TED} expression reduces to one dimension by assuming negligible axial heat flux. When this is combined with the assumption that the strain in the thick section of the beam is negligible, it implies that the Q_{TED} is determined solely from the slender beam sections. Similarly, Q_{SURF} is a fundamentally local dissipation mechanism [9] and the geometric dependence is predominantly the beam thickness [8]. Thus, both Q_{TED} and Q_{SURF} are unaffected by the main Q_{SUPP} tuning parameter, $\frac{h_L}{h_S}$.

From this is it not unreasonable to assert that a set of geometric parameters can be found that provide a Q_{TED} and Q_{SURF} in line with the highest found in the literature for a beam resonator, whilst still maintaining the same Q_{SUPP}.

5. Conclusions

It has been shown that a Q_{SUPP} value for the TMBR can theoretically be achieved of the order of those currently available in the literature and can be increased or decreased by altering the wave-speed ratio between segments. In addition, it has been reasoned that the other dominant Q contributors can be tuned with minimal effect on the achievable Q_{SUPP} value. The use of the equivalent lumped parameter model for obtaining qualitative information about TMBR systems has been validated.

The given conclusions indicate that the TMBR geometry can be a suitable choice as a MEMS resonator as a support structure for other resonant devices.

6. References

1. H. T. D. Grigg and B. J. Gallacher, “Efficient Parametric Optimisation of Support Loss in MEMS beam resonators via an enhanced Rayleigh-Ritz method”, *J. Phys. Conf. Ser.*, **382**, p. 012028 (2012)
2. Z. Hao, A. Erbil, and F. Ayazi, “An analytical model for support loss in micromachined beam resonators with in-plane flexural vibrations,” *Sensors Actuators A Phys.*, **109**, no. 1–2, pp. 156–164 (2003)
3. S. Rao, *Vibration of Continuous Systems*, John Wiley & Sons, Inc., New Jersey (2007)
4. M. Cross and R. Lifshitz, “Elastic wave transmission at an abrupt junction in a thin plate with application to heat transport and vibrations in mesoscopic systems,” *Phys. Rev. B*, **64**, no. 8, p. 085324 (2001)
5. L. Brillouin, *Wave propagation in periodic structures; electric filters and crystal lattices*. Dover Publications Inc., New York (1946)
6. D. J. Mead, “Wave propagation and natural modes in periodic systems: I. Mono-coupled systems,” *J. Sound Vib.*, **40**, pp. 1–18 (1975)
7. G. Rogers, “A diameter 300 µm Bragg reflector for acoustic isolation of resonant micro-actuators,” *Journal of Micromechanics and Microengineering*, **21**, no. 4, p. 042001 (2011)
8. H. T. D. Grigg, “The Principles and Practice of the Xylophone Bar Magnetometer”, PhD Thesis, Newcastle University, (2013)
9. T. Yang, J.Ono and M. Esashi, “Energy dissipation in submicrometer thick single-crystal silicon cantilevers,” *J. Microelectromechanical Syst.*, **11**, no. 6, p. 775–783 (2002)